14th International Conference on Structural Safety and Reliability - ICOSSAR'25
1-6 June, 2025 - Los Angeles California, USA
R. Ghanem, E. Johnson, S. Masri and A. Olivier (Eds)

PREDICTION OF AFTERSHOCK CHARACTERISTICS

MIN SHU[1] AND RUIQIANG SONG[2]

[1] Central Michigan University
Pearce Hall 111, Mount Pleasant, MI 48859, USA
shu1m@cmich.edu
https://www.cmich.edu/people/MIN-SHU

[2]Central Michigan University
song1r@cmich.edu

Key words: Aftershock, Mainshock, Earthquake, Ground motion Characteristics

Abstract. A large earthquake can trigger a series of smaller earthquakes (i.e., aftershocks) around the epicenter of the first large earthquake (i.e., mainshock). The ground motion characteristics of aftershocks can have a significant impact on collapse risk of post-mainshock structures. However, most current seismic analysis and design do not take into account aftershock risk. This study investigates the aftershock characteristics based on the Pacific Earthquake Engineering Research Center (PEER) Next Generation Attenuation (NGA) West2 (shallow crustal earthquake in active tectonic regimes) ground motion database. Since the classification of mainshock and aftershock is ambiguous and there is lack of consensus on how to define aftershocks, this study classifies the mainshocks and aftershocks by combining the Gardner and Knopoff time window and the centroid Joyner-Boore distance. To investigate the relationship between mainshock and the subsequent aftershocks with maximum magnitude, this study selected 27 MS-AS sequence events. This study finds that the distribution of magnitude differences between mainshock and the largest aftershock is highly positively skewed, indicating that the median magnitude difference is a better measure than its mean value. By using the bootstrap resampling method, the 95% confidence interval of the median magnitude difference is determined to be [0.340, 0.635], indicating that the median largest aftershock magnitude is significantly lower than its mainshock magnitude at the 5% significance level. This finding suggests that the widely accepted Bath's law (the magnitude difference between mainshock and the largest aftershock is independent of the mainshock magnitude and is approximately a constant 1.2) may significantly underestimate the magnitude of aftershocks, leading to inadequate aftershock risk assessment. This study also finds that the median largest aftershock duration may be not less than its mainshock duration at the 5% significance level and the mechanism of mainshock may be very different from those of aftershocks.

1 INTRODUCTION

A large earthquake can trigger a series of smaller earthquakes (i.e., aftershocks) around the epicenter of the first large earthquake (i.e., mainshock) because of the complex stress interaction of tectonic plates surrounding displaced fault planes after a mainshock. The rock surrounding

the epicenter of mainshock becomes dynamically unstable and the occurrence of aftershocks is considered to adjust for this dynamical instability. The seismic activity pattern that consists of a mainshock followed by aftershocks is referred to as the mainshock-aftershock (MS-AS) sequence. Recent seismic activities highlight the potential risk from aftershock hazards. The May 12, 2008, M7.9 Sichuan earthquake triggered 515 aftershock of magnitude 5.0 or greater within three weeks, resulting in 69,195 people killed, 374,177 injured, and economic losses of US$86 billion [1]. The February 27, 2010, M8.8 Chilean (Maule) earthquake incurred 217 aftershocks of magnitude 5.0 or greater within three weeks, killing at least 523 people, injuring approximately12,000, and causing economic losses of US$30 billion [2]. The March 11, 2011, M9.1 Tohoku earthquake in Japan triggered 53 aftershocks with magnitude M6.0 or above in the following three weeks. This MS-AS sequence causes approximately US$309 billion in economic losses and over 20,000 fatalities [3]. The April 25, 2015, M 7.8 Nepal earthquake incurred 30 aftershocks of magnitude 5.0 or greater within three weeks, killing at least 8,669 people and injuring 17,866 [4]. On February 6, 2023, a M7.8 earthquake struck southern Turkey near the northern border of Syria, followed by a M6.7 aftershock just 11 minutes later, and a M7.5 aftershock 9 hour later, and triggered 427 aftershocks of magnitude 4.0 or above within three weeks. The 2023 Turkey–Syria earthquakes killed at least 59,488 people and injured 121,704 people [5].

Aftershocks have the potential to pose a significant risk to life safety, cause further structural damage, hinder the reuse and repair of buildings, and increase economic losses, especially when buildings suffer to a certain level of damage during the mainshock [6,7]. The ground motion characteristics of aftershocks can have a significantly impact on the collapse risk of post-mainshock structures [8,9]. Thus, the effects of aftershocks should be taken into account in the modern seismic analysis and design of buildings. However, most current seismic analysis and design only consider mainshock and do not take into account aftershock hazards. In addition, the next generation performance-based seismic design, which aims to provide a realistic and reliable understanding of the risk of life, occupancy, and economic loss that may result from future earthquakes when designing and constructing buildings, does not account for aftershock hazards [10].

The study of aftershocks can be traced back to the 19th century. A few empirical laws in seismology have been well established to describe aftershocks rate and magnitudes. The decay of aftershock activity with time was first proposed by Fusakichi Omori in 1895 that the aftershock rate decreases roughly with the reciprocal of time after the mainshock, known as Omori's law [11]. Utsu [12] modified the Omori's law to change the decay rate, known as the Utsu-Omori law that are commonly used. The relationship between the magnitude and frequency of aftershocks typically follows the Gutenberg–Richter law, with more small aftershocks and fewer large aftershocks [13]. The difference between a mainshock and its largest aftershock generally follows the Båth law, which states that on the moment magnitude scale, the difference is independent of the mainshock magnitude and is approximately a constant 1.2 [14].

In recent years, there has been an increasing number of studies on aftershock characteristics and intensity measurements. Abrahamson and Silva [15] and Abrahamson et al. [16] built the empirical ground motion prediction models for the average horizontal component from shallow crustal earthquakes by using regression analysis to compute the median spectral accelerations and adopted an additional term to account for the difference in the medians between mainshocks and aftershocks. Das and Gupta [17] developed conditional scaling models for estimating pseudo

spectral velocity and strong motion duration of aftershocks based on the database of the 1999 Chi-Chi earthquake and regression analysis. Wooddell and Gu et al. [18] investigated the statistical properties of aftershocks in Southern California and found that several statistical features depend sensitively on the definition and identification of aftershocks. Wooddell and Abrahamson [19] defined the centroid Joyner-Boore distance as the shortest horizontal distance between the centroid of the potential aftershock rupture surface projection and the surface projection of the mainshock rupture plane, and combined it with Gardner and Knopoff time window [20] to classify the mainshocks and aftershocks. Davidsen et al. [21] proposed a generalized Omori–Utsu law for the aftershock sequences in southern California to unify the Gutenberg–Richter law, the Utsu-Omori law and the Båth law. Han et al. [22] synthesized time histories of aftershock using spectral representation and sinusoidal waves superposition and proposed that the magnitude difference between mainshock and the largest aftershock follows the beta distribution based on the 32 selected MS-AS sequences. Kim and Shin [23] built an empirical model to estimate the ratios of aftershocks to mainshocks for peak ground motion acceleration, peak ground velocity, and 5% damped pseudo spectral acceleration at various periods. Zhu et al. [24] generated the conditional mean spectrum of aftershocks by using the copula-based joint distributions of the epsilons between the mainshocks and their largest magnitude aftershocks and the Abrahamson et al. [16] ground motion prediction model. Lee et al. [25] quantified the difference in the spectral accelerations and the mean periods between mainshock and aftershock using the Japanese KiK-net database.

This study investigates ground motion characteristics of mainshock and the subsequent aftershocks with maximum magnitude based on real MS-AS sequence events. This study is organized as follows: Section 2 presents a brief description of the mainshock-aftershock sequence, Section 3 investigates the relationships of characteristics between mainshock and its largest aftershock, and Section 4 concludes the study.

2 MAINSHOCK-AFTERSHOCK SQUENCES

2.1 Dataset

This study uses the Pacific Earthquake Engineering Research Center (PEER) Next Generation Attenuation (NGA) West2 (shallow crustal earthquake in active tectonic regimes) ground motion database (PEER, n.d.) to collect the information of historical earthquake records. The PEER established in 1996, headquartered at the University of California, Berkeley, is a collaborative hub involving over 20 universities, consulting firms, and researchers from State and Federal government agencies. Their collective efforts are dedicated to advancing research in performance-based earthquake engineering across various fields such as structural and geotechnical engineering, geology/seismology, lifelines, transportation, and public policy. The PEER curates a vast collection of ground motion records from around the world. They meticulously process and validate the data, capturing essential metadata such as earthquake magnitude, site-to-source distances, faulting style, local site conditions, and other relevant engineering parameters. This comprehensive information is then made accessible to the public through an online database. Currently, there are 21,508 valid records from 599 different earthquake events in the NGA-West2 ground motion database, including 4,337 valid aftershock records from 217 aftershock events.

2.2 Mainshock-Aftershock Sequences

Since the classification of mainshock and aftershock is ambiguous and there is lack of consensus on how to define aftershocks, this study adopts the classification method proposed by Wooddell and Abrahamson [19] to classify the mainshocks and aftershocks based on the combination of the centroid Joyner-Boore distance (i.e., the shortest horizontal distance between the centroid of the potential aftershock rupture surface projection and the surface projection of the mainshock rupture plane) and the Gardner and Knopoff time window. Table 1 lists the selected values for the magnitude-dependent time and distance windows. The values are parameterized using a linear model for the distance window and a bilinear model for the time window. If an earthquake event occurs within the Gardner and Knopoff time window and the centroid Joyner-Boore distance less than a selected cutoff value, the earthquake event is classified as an aftershock event.

In this preliminary study, we focus only on the MS-AS sequences consisting of a mainshock and its subsequence aftershock of the largest magnitude. This study selects 27 sequence events, consisting of 27 mainshocks and their first largest aftershocks. Table 2 lists the basic information of selected MS-AS sequence events, including the Earthquake name, magnitude (M), and EQID which is an arbitrary unique ID assigned to each earthquake for identification in the PEER NGA-West2 Database. Table 3 lists the ground motion characteristics of the selected mainshock-aftershock sequences, including the Station Sequence Number (Station No.) which is an arbitrary unique sequence number assigned to each strong-motion, magnitude difference (ΔM) between mainshock and aftershock, and the occurrence time interval between mainshock and aftershock, mechanism and duration. In this study, the duration of ground motion record is measured by the significant duration for the time needed to build up between 5 and 95 percent of the total Arias intensity. The Arias intensity is a measure of the strength of a ground motion and is defined as the sum of all the squared acceleration values from seismic strong motion records. The descriptive statistics of ground motion characteristics of selected mainshock-aftershock sequences are listed in Table 4.

Table 1: Window Algorithm for Aftershocks

Moment Magnitude	Centroid Joyner-Boore Distance (km)	Duration Time of Sequence (days)
2.5	19.5	6
3.0	22.5	11.5
3.5	26	22
4.0	30	42
4.5	35	83
5.0	40	155
5.5	47	290
6.0	54	510
6.5	61	790
7.0	70	915
7.5	81	960
8.0	94	985

Table 2: Basic Information of the Selected Mainshock-aftershock Sequence Events

Seq. No.	Mainshock			Aftershock		
	Earthquake name	M	EQID	Earthquake name	M	EQID
1	Northwest Calif-03	5.8	11	Northern Calif-02	5.2	13
2	Hollister-01	5.6	23	Hollister-02	5.5	24
3	Managua, Nicaragua-01	6.24	31	Managua, Nicaragua-02	5.2	32
4	Friuli, Italy-01	6.5	40	Friuli, Italy-02	5.91	43
5	Imperial Valley-06	6.53	50	Westmorland	5.9	73
6	Livermore-01	5.8	53	Livermore-02	5.42	54
7	Mammoth Lakes-01	6.06	56	Mammoth Lakes-06	5.94	61
8	Irpinia, Italy-01	6.9	68	Irpinia, Italy-02	6.2	69
9	Mammoth Lakes-10	5.34	74	Mammoth Lakes-11	5.31	75
10	Coalinga-01	6.36	76	Coalinga-05	5.77	80
11	Chalfant Valley-02	6.19	103	Chalfant Valley-03	5.65	104
12	Whittier Narrows-01	5.99	113	Whittier Narrows-02	5.27	114
13	Landers	7.28	125	Big Bear-01	6.46	126
14	Kocaeli, Turkey	7.51	136	Duzce, Turkey	7.14	138
15	Northridge-01	6.69	127	Northridge-02	6.05	147
16	Northwest China-03	6.1	155	Northwest China-04	5.8	156
17	Chi-Chi, Taiwan	7.62	137	Chi-Chi, Taiwan-06	6.3	175
18	Ancona-02, Italy	4.6	182	Ancona-03, Italy	4.4	183
19	Ancona-09, Italy	4.7	189	Ancona-10, Italy	4.3	190
20	Lazio Abruzzo, Italy	5.8	91	Lazio Abruzzo (aftershock 1), Italy	5.5	225
21	Umbria Marche, Italy	6	234	Umbria Marche (aftershock 2), Italy	5.6	243
22	L'Aquila, Italy	6.3	274	L'Aquila (aftershock 1), Italy	5.6	275
23	Darfield, New Zealand	7	281	Christchurch, New Zealand	6.2	346
24	Parkfield-02, CA	6	179	21401069	5	1199
25	71336726	4.05	1221	71337451	3.73	1222
26	51215567	3.8	1248	51215571	3.49	1249
27	14383980	5.39	1002	14384052	3.8	1259

Table 3: Ground Motion Characteristics of the Selected Mainshock-aftershock Sequences

Seq. No.	Station No.	ΔM	Interval (s)	Mainshock		Aftershock	
				Mechanism	Duration (s)	Mechanism	Duration (s)
1	133	0.6	30267000	strike slip	15.4	strike slip	18.4
2	135	0.1	120	strike slip	18.7	strike slip	16.5

3	199	1.04	3000	strike slip	10.6	strike slip	8.1
4	251	0.59	11344500	Reverse	19	Reverse	23.8
5	216	0.63	48257580	strike slip	14.9	strike slip	8.8
6	469	0.38	199980	strike slip	10.3	strike slip	10.9
7	429	0.12	166620	Normal Oblique	9.6	strike slip	6.8
8	605	0.7	60	Normal	19.3	Normal	18.8
9	429	0.03	6360	strike slip	8.2	strike slip	10.1
10	156	0.59	6922620	Reverse	9.1	Reverse	7.3
11	432	0.54	540	strike slip	16.8	strike slip	19.3
12	342	0.72	245820	Reverse Oblique	5.7	Reverse Oblique	7.8
13	1388	0.82	11280	strike slip	24.5	strike slip	10.4
14	597	0.37	7516800	strike slip	37.2	strike slip	39.7
15	350	0.64	60	Reverse	15.5	Reverse	15.1
16	1386	0.3	391500	Normal	13.5	Normal Oblique	14.2
17	636	1.32	517920	Reverse Oblique	27.2	Reverse	12.2
18	3630	0.2	23760	Normal	4	Normal	3.8
19	3606	0.4	7560	strike slip	11.6	Normal	4.7
20	1637	0.3	319860	Normal	11.9	Normal	12.3
21	3616	0.4	1575780	Normal	9.3	Normal	4.8
22	1985	0.7	144840	Normal	8.9	Normal Oblique	3.5
23	3464	0.8	14800560	strike slip	34.1	Reverse Oblique	14.3
24	100052	1	86100	strike slip	71.5	strike slip	62.9
25	100005	0.32	92340	strike slip	13.6	Reverse Oblique	14.2
26	100403	0.31	2580	strike slip	17.4	strike slip	13.9
27	1318	1.59	540	Reverse Oblique	12.4	strike slip	4.5

Table 4: Descriptive Statistics of Ground Motion Characteristics of Selected Mainshock-aftershock Sequences

Variable	Mean	Std. dev.	Median	Min	Max	skew	kurtosis
Mainshock Mag.	6.01	0.94	6.06	3.8	7.62	-0.52	-0.08
Aftershock Mag.	5.43	0.86	5.6	3.49	7.14	-0.63	-0.08
ΔM	0.57	0.36	0.59	0.03	1.59	0.88	0.54
Mainshock Duration	17.41	13.37	13.6	4	71.5	2.53	7.29
Aftershock Duration	14.34	12.31	12.2	3.5	62.9	2.49	6.76
ΔD	3.08	5.95	1.8	-4.8	19.8	1.15	0.68
Interval	4.55E+06	1.10E+07	1.45E+05	60	4.83E+07	2.79	7.42

3 RELATIONSHIPS OF CHARACTERISTICS BETWEEN MAINSHOCK AND ITS LARGEST AFTERSHOCK

3.1 Relationship of Magnitude between Mainshock and Aftershock

According to Table 4, the skewness and kurtosis of magnitude difference (ΔM) between mainshock and its largest aftershock are 0.88 and 0.54, respectively, indicating that the distribution of magnitude differences between mainshock and the largest aftershock is highly positively skewed and does not obey normal distribution. The median magnitude difference is a better measure than its mean. By using the nonparametric bootstrap resampling method with 10000 bootstrap replicates, the 95% confidence interval of the median magnitude difference is determined to be [0.37, 0.70], indicating that the median largest aftershock magnitude is significantly lower than its mainshock magnitude at the 5% significance level. This finding suggests that the widely accepted Bath's law (the magnitude difference between mainshock and the largest aftershock is independent of the mainshock magnitude and is approximately a constant 1.2) may significantly underestimate the magnitude of aftershocks, leading to inadequate aftershock risk assessment.

3.2 Relationship of Duration between Mainshock and Aftershock

The skewness and kurtosis of duration difference (ΔD) between mainshock and its largest aftershock in Table 4 are 1.15 and 0.68, respectively, indicating that the distribution of duration differences between mainshock and the largest aftershock is positively skewed, and the median duration difference is a better measure than its mean. By using the nonparametric bootstrap resampling method with 10000 bootstrap replicates, the 95% confidence interval of the median duration difference is determined to be [-0.6, 4.5], indicating that the median largest aftershock duration is not less than its mainshock duration at the 5% significance level.

3.3 Relationship of Mechanism between Mainshock and Aftershock

Figure 1 presents the barchart of mainshock mechanism grouped by aftershock mechanism. We can see that the mechanism of mainshock may be very different from those of aftershocks. For example, a mainshock with a reverse oblique mechanism is likely to cause strike slip aftershocks. However, a mainshock with a reverse mechanism is likely to cause reverse aftershocks.

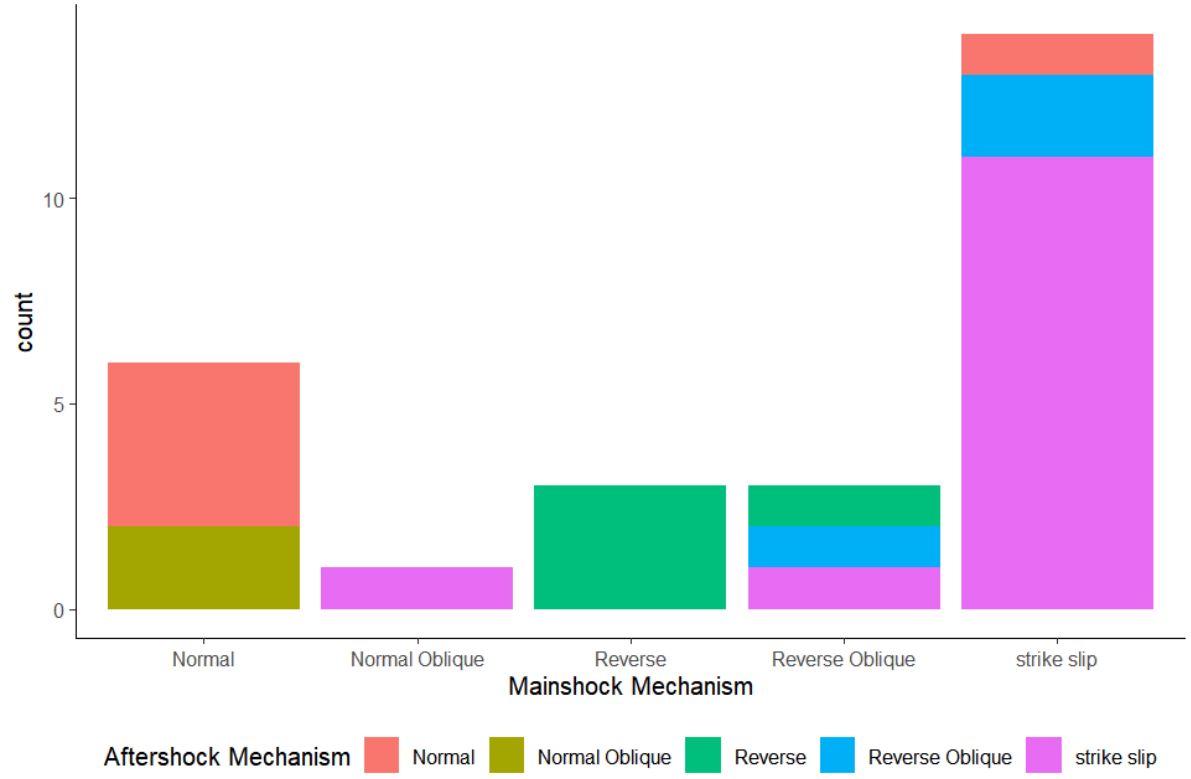

Figure 1: Barchart of Mainshock Mechanism Grouped by Aftershock Mechanism

3.4 Occurrence Interval between Mainshock and Aftershock

The descriptive occurrence interval between mainshock and aftershock is listed in Table 4. The largest aftershock may occur just within a minute of the mainshock or a year and a half after the mainshock. The mean value is 52.7 days, while the median value is about a day and a half (144840 s). The skewness and kurtosis of interval between mainshock and its largest aftershock in Table 4 are 2.79 and 7.42, respectively, indicating that the distribution of interval positively skewed, and the median value is a better measure than its mean. Based on the nonparametric bootstrap resampling method with 10000 bootstrap replicates, the 95% confidence interval of the median interval is determined to be [7560, 391500].

4 CONCLUSIONS

This study investigates ground motion characteristics of mainshock and the subsequent aftershocks with maximum magnitude based on selected 27 MS-AS sequence events from PEER NGA-West2 ground motion database. This study classifies the mainshocks and aftershocks based on the combination of the centroid Joyner-Boore distance and the Gardner and Knopoff time window. The 95% confidence interval of the median magnitude difference between mainshock and aftershock [0.37, 0.70] indicates that the widely accepted Bath's law may significantly underestimate the magnitude of aftershocks, thereby leading to inadequate aftershock risk assessment. In addition, the median largest aftershock duration may be not less than its mainshock duration at the 5% significance level. Moreover, the mechanism of

mainshock may be very different from those of aftershocks. Further, the 95% confidence interval of the median occurrence interval between mainshock and its largest aftershock is [7560s, 391500s].

REFERENCES

[1] USGS. M 7.9 - 58 km W of Tianpeng, China. https://earthquake.usgs.gov/earthquakes/eventpage/usp000g650/executive.

[2] USGS. M 8.8 - 36 km WNW of Quirihue, Chile. https://earthquake.usgs.gov/earthquakes/eventpage/official20100227063411530_30/executive.

[3] USGS. M 9.1 - 2011 Great Tohoku Earthquake, Japan. https://earthquake.usgs.gov/earthquakes/eventpage/official20110311054624120_30/executive.

[4] USGS. M 7.8 - 67 km NNE of Bharatpur, Nepal. https://earthquake.usgs.gov/earthquakes/eventpage/us20002926/executive.

[5] USGS. M 7.8 - Pazarcik earthquake, Kahramanmaras earthquake sequence. https://earthquake.usgs.gov/earthquakes/eventpage/us6000jllz/executive.

[6] Li, Y., Song, R. & Van De Lindt, J. W. Collapse Fragility of Steel Structures Subjected to Earthquake Mainshock-Aftershock Sequences. *J. Struct. Eng.* (2014) **140**:04014095.

[7] Song, R., Li, Y. & Van de Lindt, J. W. Loss estimation of steel buildings to earthquake mainshock–aftershock sequences. *Struct. Saf.* (2016) **61**:1–11.

[8] Song, R. RISK ANALYSIS OF STEEL FRAME BUILDINGS DUE TO EARTHQUAKE MAINSHOCK-AFTERSHOCK SEQUENCES. (Michigan Technological University, Houghton, Michigan, 2014). doi:10.37099/mtu.dc.etd-restricted/262.

[9] Song, R., Li, Y. & van de Lindt, J. W. Impact of earthquake ground motion characteristics on collapse risk of post-mainshock buildings considering aftershocks. *Eng. Struct.* (2014) **81**:349–361.

[10] FEMA. *Seismic Performance Assessment of Buildings, Volume 1 -- Methodology*. https://femap58.atcouncil.org/reports (2018).

[11] Omori, F. On the After-shocks of Earthquakes. *J. Coll. Sci. Imp. Univ. Jpn.* (1894) **7**:111–200.

[12] Utsu, T. A statistical study of the occurrence of aftershocks. *Geophys. Mag.* (1961) **30**: 521–605.

[13] Gutenberg, B. & Richter, C. F. Frequency of earthquakes in California. *Bull. Seismol. Soc. Am.* (1944) **34**:185–188.

[14] Båth, M. Lateral inhomogeneities of the upper mantle. *Tectonophysics* (1965) **2**:483–514.

[15] Abrahamson, N. & Silva, W. Summary of the Abrahamson & Silva NGA Ground-Motion Relations. *Earthq. Spectra* (2008) **24**:67–97.

[16] Abrahamson, N., Silva, W. J. & Kamai, R. Summary of the ASK14 Ground Motion Relation for Active Crustal Regions. *Earthq. Spectra* (2014) **30**:1025–1055.

[17] Das, S. & Gupta, V. K. Scaling of response spectrum and duration for aftershocks. *Soil Dyn. Earthq. Eng.* (2010) **30**:724–735.

[18]Gu, C., Schumann, A. Y., Baiesi, M. & Davidsen, J. Triggering cascades and statistical properties of aftershocks. *J. Geophys. Res. Solid Earth* (2013) **118**:4278–4295.
[19]Wooddell, K. E. & Abrahamson, N. A. Classification of Main Shocks and Aftershocks in the NGA-West2 Database. *Earthq. Spectra* (2014) **30**: 1257–1267.
[20]Gardner, J. K. & Knopoff, L. Is the sequence of earthquakes in Southern California, with aftershocks removed, Poissonian? *Bull. Seismol. Soc. Am.* (1974) **64**:1363–1367.
[21]Davidsen, J., Gu, C. & Baiesi, M. Generalized Omori–Utsu law for aftershock sequences in southern California. *Geophys. J. Int.* (2015) **201**:965–978.
[22]Han, R., Li, Y. & van de Lindt, J. Assessment of Seismic Performance of Buildings with Incorporation of Aftershocks. *J. Perform. Constr. Facil.* (2015) **29**:04014088.
[23]Kim, B. & Shin, M. A model for estimating horizontal aftershock ground motions for active crustal regions. *Soil Dyn. Earthq. Eng.* (2017) **92**:165–175.
[24]Zhu, R., Lu, D., Yu, X. & Wang, G. Conditional Mean Spectrum of Aftershocks. *Bull. Seismol. Soc. Am.* (2017) **107**:1940–1953.
[25]Lee, H., Park, H.-J. & Kim, B. Differences between main shock and aftershock ground motions derived from the Japanese KiK-net database. *Soil Dyn. Earthq. Eng.* (2020) **138**: 106325.